

Production and transport modelling of Po-210 in DEMO reactor

P. Chiovaro¹, A. Quartararo¹, S. Ciattaglia², P.A. Di Maio¹, S. Basile¹, I. Moscato^{1,2}, G.A. Spagnuolo², F. Moro³

¹Department of Engineering, University of Palermo, Viale delle Scienze, Ed. 6, 90128 Palermo, Italy

²Fusion Technology Department – Programme Management Unit, EUROfusion Consortium, Boltzmannstraße 2, 85748 Garching, Germany

³Department of Fusion and Technology for Nuclear Safety and Security, ENEA C. R. Frascati, via E. Fermi 45, 00044 Frascati (Roma), Italy

E-mail: pierluigi.chiovaro@unipa.it

November 2021

Abstract. One of the generic designs of the nuclear fusion DEMO reactor proposed by the EUROfusion consortium foresees the development of a tritium Breeding Blanket (BB) relying on the use of the liquid-metal PbLi eutectic alloy as both neutron multiplier and tritium breeder, namely the Water-Cooled Lithium Lead (WCLL) BB, whose strengths and weaknesses are well known. This paper focuses the attention on one of the possible disadvantages of such a technology: the production of the high radiotoxic radionuclide ^{210}Po , which could become a safety issue to be accounted for. The ^{210}Po concentration within the PbLi circuit has been assessed by solving a modified version of Bateman's equations to consider the alloy circulation, so a one-dimensional convective fluid-dynamic model has been set up. Nuclear quantities have been evaluated by Monte Carlo neutron transport analyses using MCNP code and adopting a fully heterogeneous model of DEMO equipped with the WCLL BB. Moreover, rough sensitivity analyses have been performed to assess the influence on the results of the uncertainties related to the ^{209}Bi radiative-capture cross section and the initial concentration of this nuclide which is present in the PbLi as an impurity. Results obtained have been critically discussed and some safety issues have been addressed to evaluate the possible hazard in case of a leak of PbLi accident.

Keywords: Neutronics, Fluid-dynamics, Breeding Blanket, ^{210}Po , DEMO

Submitted to: *Nucl. Fusion*

1. Introduction

The Roadmap to Fusion Electricity Horizon 2020 [1] foresees a comprehensive design study of a DEMOnstration Fusion Reactor (DEMO), based on a D-T plasma, with the aim of feeding into the grid several hundred MWs of net electricity getting the tritium self-sufficiency [2]. The DEMO component which will convert the nuclear power and will breed tritium is called Breeding Blanket (BB).

One of the generic designs of the nuclear fusion Demo reactor proposed by the EUROfusion consortium is equipped with the Water-Cooled Lithium Lead (WCLL) BB, that relies on the eutectic alloy Pb–15.8Li (PbLi from now on) as breeder/multiplier system, pressurized water as coolant, and EUROFER as structural material [3, 4] Many studies dealt with the strengths and weaknesses of this project [5, 6] and, among the identified problems, this paper focuses the attention on the production of the highly radiotoxic radionuclide ^{210}Po . Such a nuclide can be produced within the PbLi by neutron interactions with ^{209}Bi (100% abundance in natural Bismuth and present as an impurity in the alloy) and with ^{208}Pb by successive captures and decays both via the ^{209}Bi formation and directly by ^{210}Pb formation. ^{210}Po is almost a full α emitter (5.305 MeV) with a relatively short half-life of 138 d, so it is not a concern for the reactor decommissioning but its inventory could become a safety issue to be accounted for workers in case of chronic releases as well as the population in case of a major accident like a PbLi circuit pipe break.

In order to assess the ^{210}Po concentration within the PbLi circuit, a MATLAB [7] one-dimensional convective fluid-dynamic model has been set up encompassing both the liquid metal flow and the production and burning of the involved isotopes. As far as the nuclear quantities are concerned, they have been evaluated by Monte Carlo neutron transport analyses adopting MCNP-5.1.6 code [8] along with the transport cross section library JEFF3.3 [9] and the activation libraries TENDL-19 [10] to take into account ^{209}Bi , ^{210}Bi and ^{210}Po and lldos [8] for ^{209}Pb and ^{210}Pb .

In the following paragraph, the physical-mathematical model set-up is described, in section 3 neutronic results are reported, in section 4 the results obtained in terms of nuclides inventories are shown together with a sensitivity analysis assessing the influence of the uncertainties on the ^{209}Bi radiative-capture cross section and the initial concentration of this nuclide. Section 5 is dedicated to some rough safety observations related to ^{210}Po and finally, in the last section, conclusions on the outcomes of the study are drawn.

2. Description of the mathematical model

In order to show the procedure set-up to assess the concentration of ^{210}Po in the PbLi circuit, it is important to clarify how such an isotope is produced. Figure 1 shows the chains of neutron radiative captures that is the (n, γ) reactions and decays, β and α , leading to the formation of ^{210}Po within the PbLi.

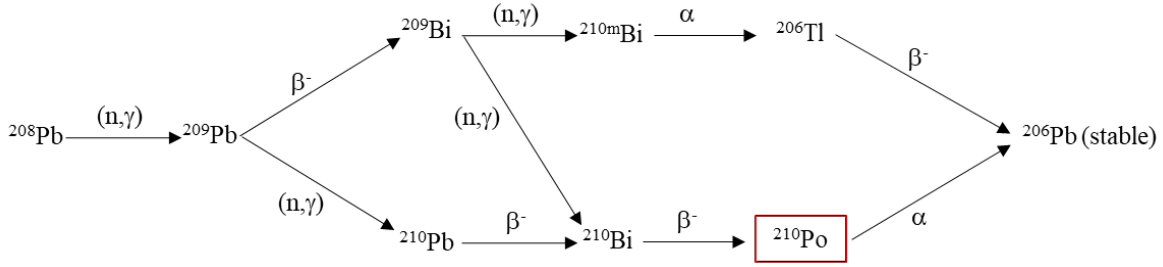


Figure 1: Scheme of polonium production in PbLi.

As it can be observed, two channels lead to ^{210}Po starting from ^{208}Pb , the first is characterized by the production of ^{209}Bi and the second by the production of ^{210}Pb . More precisely, ^{209}Bi (n, γ) reaction has a branch leading to the metastable isomer ^{210m}Bi (with a very long half-life of $3.3 \cdot 10^6$ y) which does not produce ^{210}Po . The half-lives of the radioactive isotopes above introduced are summarized in table 1 [11].

Table 1: Half-lives of the considered radioactive isotopes.

Isotope	$T_{1/2}$ [s]
^{208}Pb	Stable
^{209}Pb	$1.171080 \cdot 10^4$
^{210}Pb	$7.032528 \cdot 10^8$
^{209}Bi	Stable
^{210}Bi	$4.330368 \cdot 10^5$
^{210}Po	$1.195569 \cdot 10^7$

The branching ratio between the reactions ^{209}Bi (n, γ) ^{210}Bi and ^{209}Bi (n, γ) ^{210m}Bi is about 2/3 [12, 13], but it is to be noted that cross section libraries show not negligible discrepancies on this value so that it represents a source on uncertainty for the calculation which is to be taken into account.

The scheme of figure 1 shows that to determine the ^{210}Po concentration along the PbLi circuit the dynamic behaviour of the involved isotopes must be evaluated. Moreover, since the PbLi flows in the in-vessel components (where it is irradiated) and ex-vessel piping of the aforementioned circuit, the convective transport of the isotopes and their irradiation histories have to be considered. So, a modified version of Bateman's equations has been set up considering a one-dimensional fluid-dynamic model as follows:

$$\left\{ \begin{array}{l}
\frac{\partial N_{Pb-208}(x, t)}{\partial t} + u(x, t) \frac{\partial N_{Pb-208}(x, t)}{\partial x} = -r_{Pb-208}^{rem}(x, t) N_{Pb-208}(x, t) \\
\frac{\partial N_{Pb-209}(x, t)}{\partial t} + u(x, t) \frac{\partial N_{Pb-209}(x, t)}{\partial x} = r_{Pb-208}^{n, \gamma}(x, t) N_{Pb-208}(x, t) \\
\quad - [r_{Pb-209}^{rem}(x, t) + \lambda_{Pb-209}] N_{Pb-209}(x, t) \\
\frac{\partial N_{Pb-210}(x, t)}{\partial t} + u(x, t) \frac{\partial N_{Pb-210}(x, t)}{\partial x} = r_{Pb-209}^{n, \gamma}(x, t) N_{Pb-209}(x, t) \\
\quad - [r_{Pb-210}^{rem}(x, t) + \lambda_{Pb-210}] N_{Pb-210}(x, t) \\
\frac{\partial N_{Bi-209}(x, t)}{\partial t} + u(x, t) \frac{\partial N_{Bi-209}(x, t)}{\partial x} = \lambda_{Pb-209} N_{Pb-209}(x, t) \\
\quad - r_{Bi-209}^{rem}(x, t) N_{Bi-209}(x, t) \\
\frac{\partial N_{Bi-210}(x, t)}{\partial t} + u(x, t) \frac{\partial N_{Bi-210}(x, t)}{\partial x} = \gamma r_{Bi-209}^{n, \gamma}(x, t) N_{Bi-209}(x, t) \\
\quad + \lambda_{Pb-210} N_{Pb-210}(x, t) \\
\quad - [r_{Bi-210}^{rem}(x, t) + \lambda_{Bi-210}] N_{Bi-210}(x, t) \\
\frac{\partial N_{Po-210}(x, t)}{\partial t} + u(x, t) \frac{\partial N_{Po-210}(x, t)}{\partial x} = \lambda_{Bi-210} N_{Bi-210}(x, t) \\
\quad - [r_{Po-210}^{rem}(x, t) + \lambda_{Po-210}] N_{Po-210}(x, t)
\end{array} \right. \quad (1)$$

In the set of equations (1), the symbol N is used to indicate the concentration of the isotope labelled by the subscript, u is the PbLi speed, λ_s the decay constants, γ the ^{209}Bi radiative capture reaction yield and the r_s are the following quantities:

$$\begin{aligned}
r_s^{rem}(x, t) \cong r_s^{rem}(x_i, t) &= \frac{1}{V_i} \int_0^{+\infty} \int_{4\pi} \int_{V_i} [\sigma_s^{n, \gamma}(\underline{x}, E) + \sigma_s^{n, 2n}(\underline{x}, E) \\
&\quad + \sigma_s^{n, p}(\underline{x}, E) + \sigma_s^{n, \alpha}(\underline{x}, E) + \dots] \varphi(\underline{x}, \underline{\Omega}, E, t) dV d\underline{\Omega} dE, \quad (2)
\end{aligned}$$

which is the isotope removal rate due to all the transmutation reactions for a unit density, and

$$r_s^{n, \gamma}(x, t) \cong r_s^{n, \gamma}(x_i, t) = \frac{1}{V_i} \int_0^{+\infty} \int_{4\pi} \int_{V_i} \sigma_s^{n, \gamma}(\underline{x}, E) \varphi(\underline{x}, \underline{\Omega}, E, t) dV d\underline{\Omega} dE, \quad (3)$$

which is the neutron absorption rate of the isotope for a unit density.

Symbols in (2) and (3) have the usual meaning, so σ_s are microscopic cross sections, φ is the angular flux and V_i is the generic sub-volume of the calculation domain. The PbLi speed, u , has been calculated all along the circuit using the nominal mass flow rate and the dimensions of the hydraulic structures evaluated taking into account the 2019 design of the WCLL BB [14] and the 2020 design of the PbLi loop [15]. In this

regard, it is noted that the field variables, which are the isotope concentrations, have been considered as passive scalars.

As far as the boundary conditions on the spatial variable are concerned, they are imposed by the occurrence that the PbLi flows in a closed circuit and so $N(0, t) = N(L, t) \forall t$, where L is the circuit length. Regarding the initial conditions, they are reported in table 2 [16].

Table 2: Initial concentrations of the considered isotopes.

Isotope	$N(\mathbf{x}, 0) [\text{cm}^{-3}]$
^{208}Pb	$1.53380 \cdot 10^{22}$
^{209}Pb	0
^{210}Pb	0
^{209}Bi	$5.84404 \cdot 10^{18}$
^{210}Bi	0
^{210}Po	0

At this point, it is important to note that both theoretical considerations and preliminary calculations allow simplifying the problem described by (1). Firstly, the ^{208}Pb burn-up can be neglected due to the substantial abundance of ^{208}Pb in the PbLi ($\approx 44.6\%$) and the very high time constant by which it is depleted. Indeed, analyses performed with a frozen velocity field showed that the spatial average of such time constant (the inverse of the removal rate) has an order of magnitude of a few thousand years in the DEMO nominal operative scenario. Second, the channel of ^{210}Po production via ^{210}Pb is negligible because of the short half-life of ^{209}Pb (3.253 h), which makes the ^{210}Pb production not so relevant and the long half-life of ^{210}Pb (22.3 y) which is comparable with the BB life, as observed in [17]. Of course, also this assumption has been confirmed by preliminary analyses. In light of these considerations, to solve the problem, it is possible to simplify the set of equations (1) in the following way:

$$\left\{ \begin{array}{l} \frac{\partial N_{Pb-209}(x, t)}{\partial t} + u(x, t) \frac{\partial N_{Pb-209}(x, t)}{\partial x} = r_{Pb-208}^{n, \gamma}(x, t) N_{Pb-208}^0 \\ \quad - [r_{Pb-209}^{rem}(x, t) + \lambda_{Pb-209}] N_{Pb-209}(x, t) \\ \frac{\partial N_{Bi-209}(x, t)}{\partial t} + u(x, t) \frac{\partial N_{Bi-209}(x, t)}{\partial x} = \lambda_{Pb-209} N_{Pb-209}(x, t) \\ \quad - r_{Bi-209}^{rem}(x, t) N_{Bi-209}(x, t) \\ \frac{\partial N_{Bi-210}(x, t)}{\partial t} + u(x, t) \frac{\partial N_{Bi-210}(x, t)}{\partial x} = \gamma r_{Bi-209}^{n, \gamma}(x, t) N_{Bi-209}(x, t) \\ \quad - [r_{Bi-210}^{rem}(x, t) + \lambda_{Bi-210}] N_{Bi-210}(x, t) \\ \frac{\partial N_{Po-210}(x, t)}{\partial t} + u(x, t) \frac{\partial N_{Po-210}(x, t)}{\partial x} = \lambda_{Bi-210} N_{Bi-210}(x, t) \\ \quad - [r_{Po-210}^{rem}(x, t) + \lambda_{Po-210}] N_{Po-210}(x, t) \end{array} \right. \quad (4)$$

where N_{Pb-208}^0 is the initial concentration of ^{208}Pb .

3. Neutronic analyses

To assess the nuclear quantities r_s shown in (2) and (3), a point kinetic assumption has been done for the neutron flux, φ , so that its functional form has been modelled as the product of an amplitude function, I , depending on time only, and a shape function ϕ , such that $\varphi(\underline{x}, \underline{\Omega}, E, t) = I(t) \phi(\underline{x}, \underline{\Omega}, E)$. Then, I has been considered the same periodic function as the DEMO fusion power one normalized to its maximum value.

In particular, the considered DEMO duty cycle is characterized by a sequence of pulses, each one comprises a 100 s ramp-up transient, a 7200 s -long flat-top phase, a ramp-down transient of 100 s, and a 600 s dwell phase [18]. The amplitude function corresponding to the considered DEMO duty cycle is depicted in figure 2.

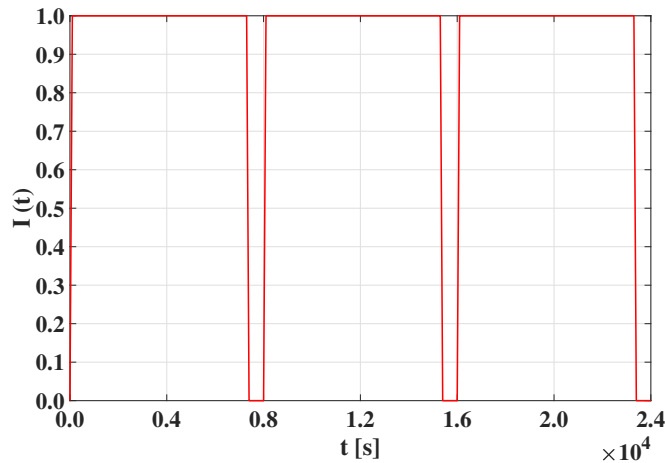


Figure 2: Amplitude time function.

As a consequence of this assumption, the quantities r_s have been calculated under a steady-state condition, applying then $I(t)$ as amplitude function. Results have been normalized using a neutron yield of $7.095 \cdot 10^{20}$ n/s which is related to the plasma flat-top phase and corresponds to a fusion power of 1998 MW, as in [19].

A fully heterogeneous MCNP model of the 2018 design of the WCLL DEMO developed at ENEA Frascati (extensively described in [19]) has been used together with a peculiar neutron source simulating the D-T plasma. Regarding the material compositions, EUROfusion recommendations have been pursued [16]. Figure 3 shows a detail of a poloidal – radial section of the model highlighting the Outboard and the Inboard segment of the WCLL BB.

The BB is composed of Breeder Units (BUs) to be considered elementary cells replicated along the poloidal direction, in particular, the OB segments are articulated in 104 BUs and the IB ones in 94 BUs [19]. Both the OB and IB segments present two irregular volumes at their poloidal limits which are filled with PbLi. Furthermore, the WCLL BB design foresees inlet and outlet PbLi manifolds to drive the flow, as clarified later in the paper.

Regarding the BB, neutronic analyses have been performed in all the PbLi domains

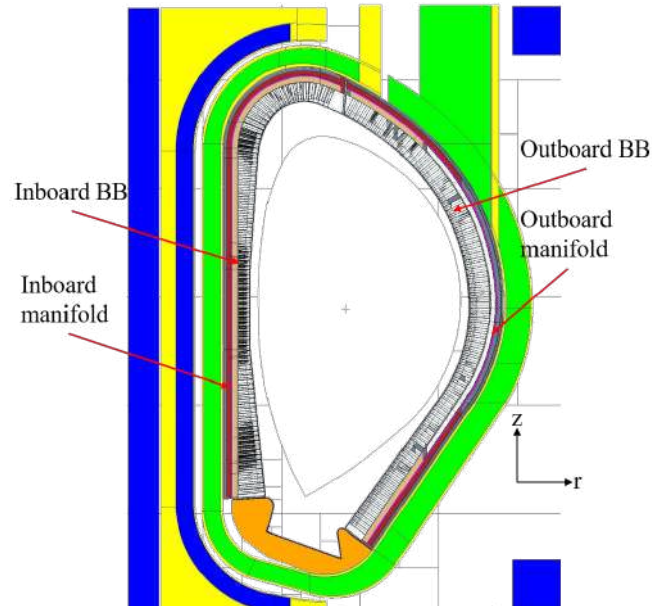


Figure 3: Detail of a poloidal – radial section of the WCLL DEMO model.

taking into account each BU and the poloidal limit volumes as well. Regarding the manifold, 29 and 31 non-overlapping poloidal segments have been considered, respectively for the IB and OB, for the calculations. Figure 4 shows the poloidal distribution of total flux during the plasma flat-top phase, reporting the values at the centre of mass of every PbLi volume. Both the OB segments, the Lateral (LOB, figure 4a) and the Central one (COB, figure 4b) have been considered, so it is possible to appreciate an albeit slight shift of the maximum values of the flux towards the equatorial zone from the left segment to the central one. In this regard, it is worth mentioning that in the OB segments the higher flux values are located in the sub-equatorial region, while the higher Neutron Wall Loading (NWL) is located around the equatorial region [19]. This discrepancy probably depends on the different poloidal discretization adopted in the two works, as demonstrated by a simple rearrangement of the results obtained for the neutron flux. This is somehow confirmed also in [20], where the profile of the NWL is evaluated using a finer poloidal segmentation than [19] and is quite flat in the region of interest. Furthermore, it is easy to deduce that the mean flux is higher in the OB than in the IB and also that the maximum value of the flux is located in the equatorial zone of the IB. This latter finding appears, again, in contrast with the poloidal profiles of the NWL in DEMO [19, 20] and this together with the previous observations leads to a more general consideration. Indeed, it seems that the common practice of using the distribution of the NWL to scale quantities related to the flux should be adopted with caution.

Figure 4c reports, on a suitable scale, the flux poloidal distribution in both the IB and LOB manifolds and shows the same behaviour as that evaluated in the blanket. As it can be noted, the neutron flux is lower in the manifolds than in the blanket but not to such an extent that the transmutation of the isotopes of interest can be considered

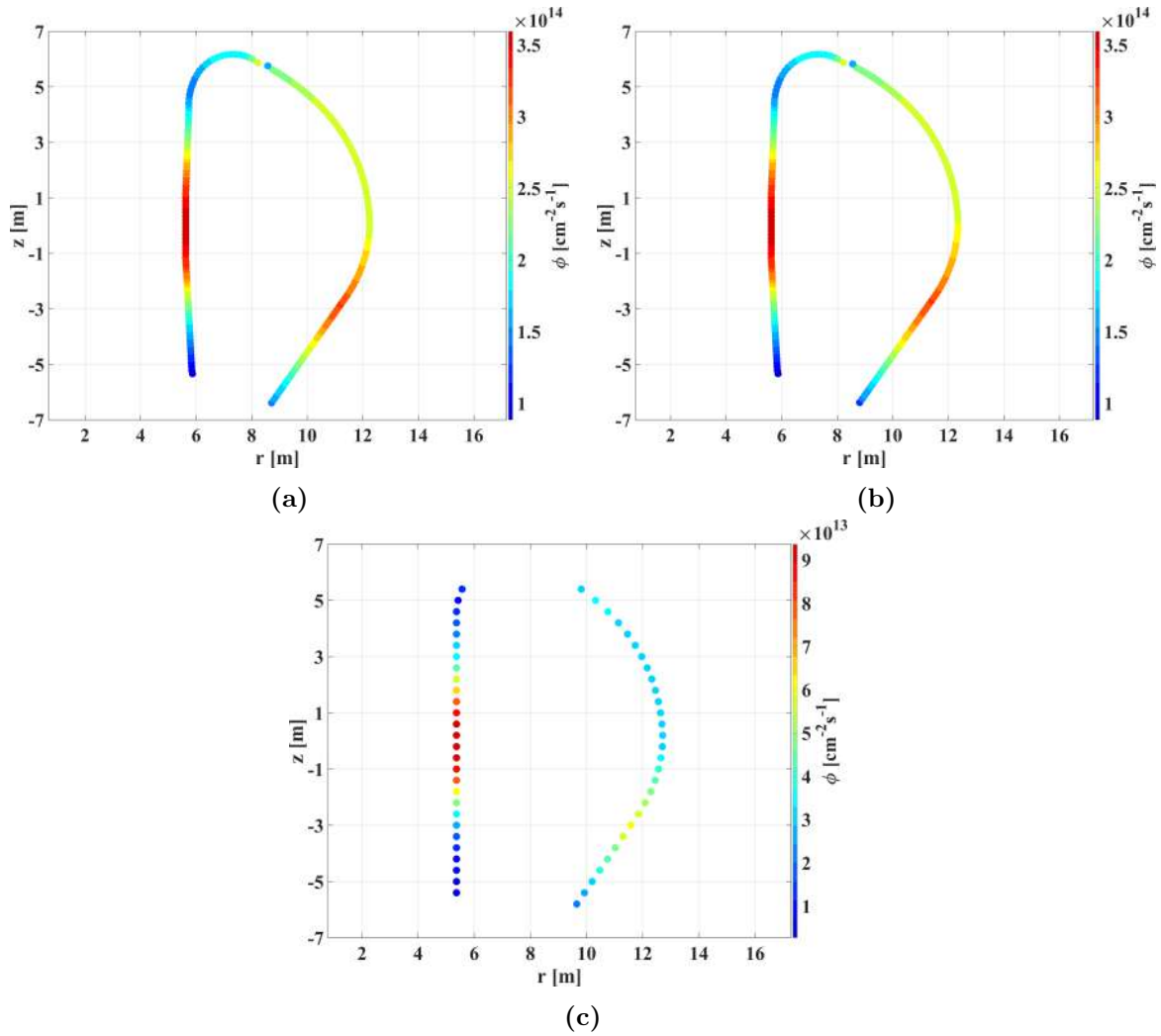


Figure 4: Neutron flux distribution on IB and LOB, (a), IB and COB, (b), and IB and LOB manifolds, (c).

negligible. For the sake of simplicity, the results related to the quantities r_s are not reported, since their spatial distributions are similar enough to the flux ones.

4. Transport analyses

To assess the distribution of ^{210}Po and the other considered isotopes concentrations along the DEMO PbLi circuit, as already mentioned, a 1D fluid-dynamic mathematical model represented by the set of equations (4) has been set up considering both the in-vessel and ex-vessel portions of the circuit.

4.1. Description of the PbLi circuit

The PbLi circuit is divided into 6 independent loops, 4 for the OB and 2 for the IB. In each loop, the various blanket segments are fed in parallel, with the inlet located at the

bottom and the outlet at the top. A 3D model of the PBLI loops is depicted in figure 5.

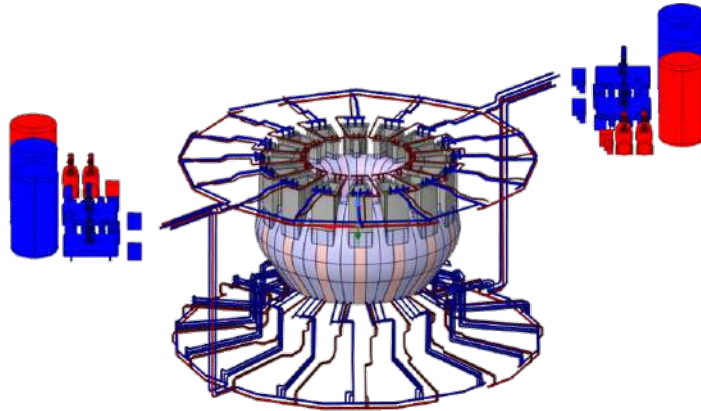


Figure 5: 3D view of outboard (blue) and inboard (red) PbLi loops.

Each BB segment is equipped with two concentric rectangular-shaped spinal manifolds (the inlet manifold is the inner one) that extend along the entire poloidal direction of the blanket. As an example, figure 6a shows the PbLi large-scale poloidal motion in a COB blanket segment.

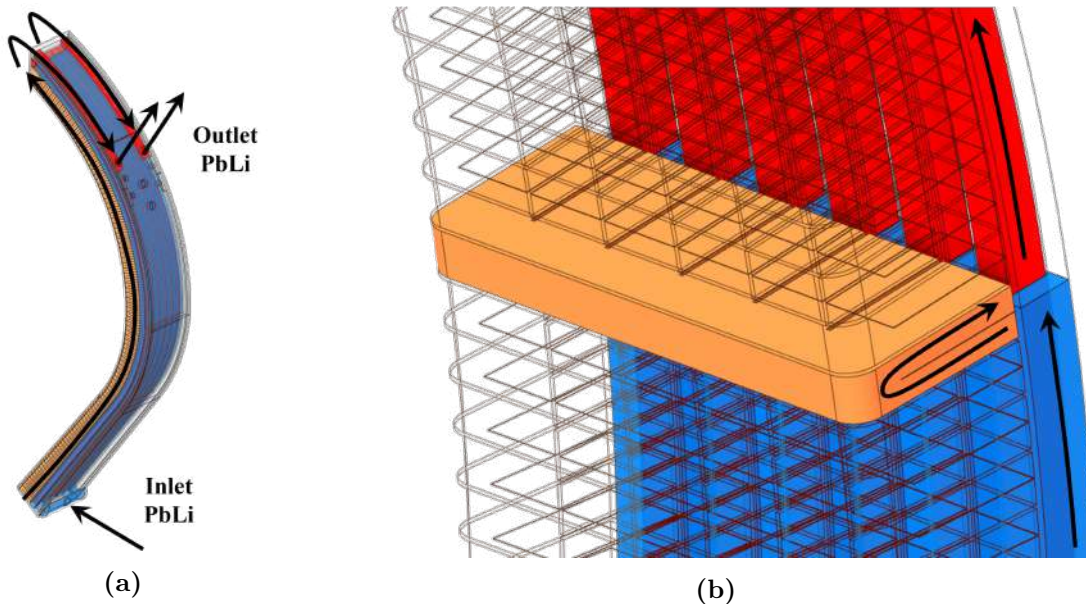


Figure 6: Schematic overview of PbLi large-scale motion inside the COB circuit, (a), and detail of the PbLi flow inside the inlet manifold (in blue), the BU (in orange), and the outlet manifold (in red), (b).

The PbLi enters the lower part of each BU from orifices present in their backplate, flows radially towards the first wall, therefore it rises poloidally and then returns radially back in the upper part of the BUs to exit from other orifices in the backplate. This

serpentine motion inside the BUs is made possible by the specific layout of stiffening and baffle plates (figure 6b).

It is important to note that the BUs are fed in parallel, so, along its circuit, the PbLi is irradiated in the manifolds (where the neutron flux is lower) and only once per cycle inside the BUs (where the neutron flux is quite high).

Considering the PbLi mass flow rates for the different IB and OB loops reported in [15], and supposing a uniform distribution of the PbLi mass flow rates both among the blanket segments and, in turn, among the different BUs, it is possible to have an estimate of the PbLi transit time inside each one of the 104 OB BUs and the 94 IB BUs. It is worth noting that, since each BU has a different geometry, significantly different transit times are obtained, as depicted in figure 7.

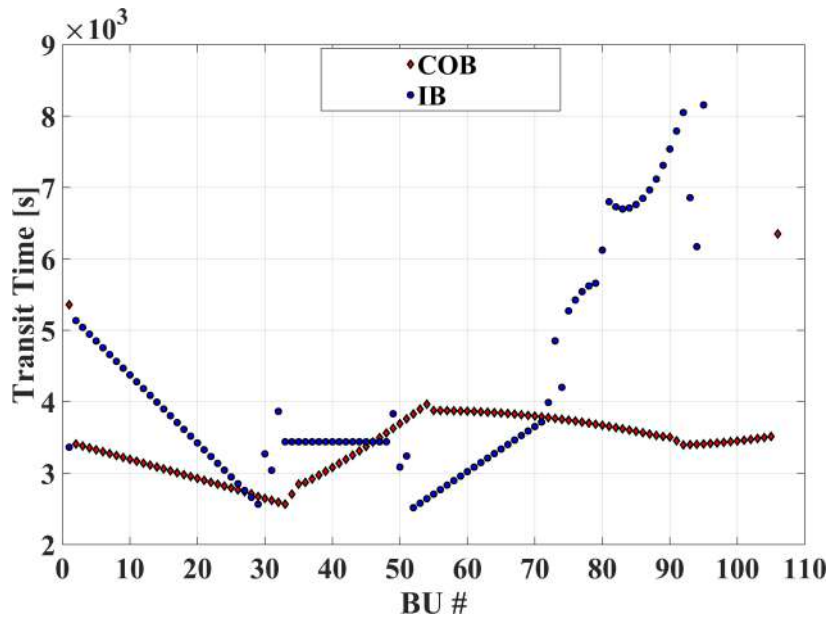


Figure 7: PbLi transit time inside each BU (for IB and COB). BUs are numbered from bottom to top.

The average transit times inside BUs, BB manifolds, and ex-vessel components of the PbLi loops are summarized in table 3, resulting in ≈ 12 circulations of PbLi per day for the IB loops and ≈ 15 circulation per day for the OB loops.

Table 3: Average transit times (in seconds) for BUs, BB manifold, and ex-vessel components.

	Transit time BUs	Transit time Manifolds	Transit time ex-vessel	Total transit time
OB	3432	1389	1021	5842
IB	4233	1628	1520	7381

4.2. Description and validation of the implemented numerical method

Finding a solution for the set of equations (4) inside the complex geometrical domain described in section 4.1 is not straightforward. This is due to the multiscale nature of the problem that requires integrating the equations over the several years of the BB lifetime, while capturing the details related to the pulsed operation, needing timescales of the order of few minutes. To overcome this issue a different approach with reference to an analogous work [21] has been considered and a dedicated numerical method has been developed, with the aim to provide accurate results in a reduced amount of time, as described in the following.

In particular, the modified Bateman's equation for the nuclear species s of equation (4) can be written in the following compact form

$$\frac{\partial N_s(x, t)}{\partial t} + u(x, t) \frac{\partial N_s(x, t)}{\partial x} = \sum_{j=1}^M a_j(x, t) N_j(x, t) + b(x, t), \quad (5)$$

where the coefficients $a_j(x, t)$ account for the λ_s and r_s values of equation (4), $b(x, t)$ is different to zero only for the ^{209}Pb equation, where a source term depending on the concentration of ^{208}Pb appears, and M is the number of nuclear species considered (here equal to 4). By adopting the method of characteristics, this set of Partial Differential Equations (PDEs) can be easily reduced to a set of Ordinary Differential Equations (ODEs) of the form

$$\frac{dN_s(x_0, t)}{dt} = \sum_{j=1}^M a_j(x_0, t) N_j(x_0, t) + b(x_0, t), \quad (6)$$

by performing a suitable change of variables. The link between equations (5) and (6) is provided by the characteristic equation

$$\frac{dx}{dt} = u(x, t), \quad (7)$$

whose general solution depends on the constant of integration x_0 , appearing as parameter in (6). Adopting this approach, it is sufficient to perform an integration in time (and not in space), but the knowledge of $N_s(x, t)$ requires to solve (6) for any value of the parameter x_0 . The method of characteristics allows to solve the original set of equations in a Lagrangian framework, i.e., equation (6) follows the evolution in time of a generic particle starting from the position x_0 at time $t = 0$ along its trajectory, determined by the solution of (7).

The adoption of this approach offers several advantages with respect to the numerical solution of (5): the time-step is not constrained to Courant-Friedrichs-Lewy (CFL) condition, it is possible to take advantage of the several optimized ODE solvers implemented in MATLAB, and it is straightforward to exploit parallel computing, since

each value of x_0 defines an equation (6) that can be solved independently from all the others, in view of the fact that there are no interactions among the different particles.

Once a solution of (6) is found in (x_0, t) , it is possible to perform an additional change of variables to the original coordinates (x, t) , exploiting again the characteristic equation (7), thus allowing to reconstruct the solution in an Eulerian framework.

The procedure described above, which will be referenced as Lagrangian-Eulerian (LE) approach from now on, has been applied to find the concentration of the generic species $N_s(x, t)$ under two simplifying assumptions. First, the complex PbLi circuits for IB and OB described in section 4.1 have been reduced to two independent closed loops of three components in series: a single equivalent BU, an equivalent manifold, and the ex-vessel PbLi components. Each component has been characterized by average values of PbLi velocity and transit time (the values of table 3 have been adopted), length, and r_s , as well as by its total volume. Second, the velocities $u(x, t)$ of equation (5) have been supposed to be only a function of space, i.e. a PbLi fluid-dynamics steady-state condition has been considered.

To numerically solve equation (4) adopting the LE approach, a discrete number P of values x_0 has been considered. For each of them, equation (6) has been integrated in time with a Dormand-Prince method of order 5 [22]. Finally, the results obtained have been interpolated over an Eulerian grid of G nodes. Albeit not mandatory, it has been chosen $G = P$ for simplicity.

Indeed, the LE approach has been thoroughly tested to assess the independence of the results on time-step size and values of P . It has been moreover checked the influence of the relative position between the BU and the manifold components inside the three-component loop. For sake of brevity, the results obtained are herewith synthetically reported:

- concerning the time-step size, a dedicated sensitivity analysis has been performed on a single Lagrangian particle starting at a given x_0 value. The results obtained showed how at least 50 time-steps are required for each pulse to obtain a maximum error on concentration below 0.5% with respect to asymptotic estimations (obtained with several thousand steps for each pulse). Moreover, it has been shown how adopting different time steps for flat-top and dwell phases could significantly improve the quality of the results with a limited increase of the overall computational cost;
- regarding the number P of discrete x_0 values, a dedicated sensitivity analysis showed that a good convergence is already obtained with $P = 30$.
- inverting the relative position of the BU and the manifolds, a negligible difference is observed on the final ^{210}Po concentration inside the circuits.

Finally, the LE approach has been validated against the results reported in [23]. In particular, the 6 Full Power Years (FPY) irradiation schedule scenario has been considered with consistent values of fusion neutron source intensity at different ^{209}Bi initial concentrations. The scenario has been simulated considering the BB as composed

of a single equivalent BU with no PbLi circulation (manifolds and ex-vessel components have been neglected, as in [23]). The outcomes of the analyses are reported in figure 8, in terms of ^{210}Po concentration after 6 FPY operation. As it can be noted, the results obtained with the proposed method are in line with the findings of [23], reported in figure considering different cross section libraries.

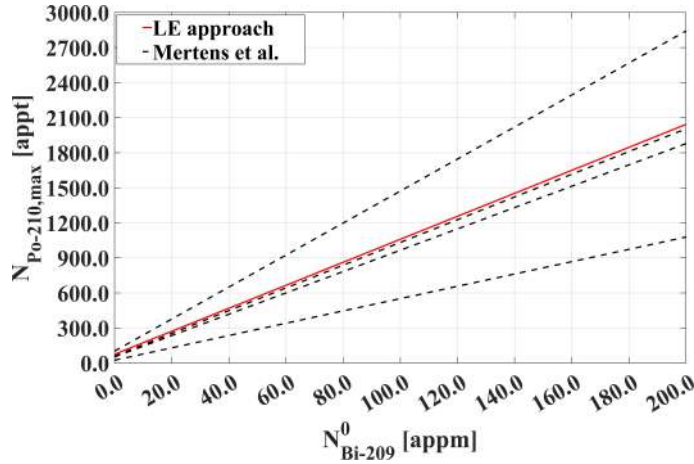


Figure 8: Comparison between results obtained with the LE approach (in red) and the results of [23] obtained with different cross section libraries (dashed lines).

4.3. Results

Transport analyses have been performed under the hypothesis of a pulsed DEMO scenario without considering the reactor availability factor. More precisely, a time interval of 6 years has been investigated in such a way to collect a budget of neutrons almost equal to that obtained considering an expected life of 6 FPY for the blanket. Of course, this working scenario could be thought of as that of a fusion power plant.

Figure 9a shows the time behaviour of the isotope concentrations in the whole IB (similar results are obtained for the OB) and it highlights how ^{210}Po gets essentially saturated in about 2 years, ^{209}Pb in approximately 1 month, and ^{210}Bi in a few pulses. Differently from the other species, ^{209}Bi grows very slightly, deviating just a little from its initial concentration. Figure 9b shows the ^{210}Po concentrations in the IB and OB, making clear that the behaviour is almost the same in the two sections of the blanket, even if the concentration is always slightly higher in the IB. This is due to the greater transit times in the in-vessel section of the IB in which, then, PbLi is irradiated longer. Furthermore, it is observed that also the transit time in the ex-vessel section in the IB is greater than in the OB but both are much shorter than the ^{210}Po half-life and therefore it is not possible to appreciate a significant difference in the removal of the isotope due to the decay in the ex-vessel section of two circuits.

Some additional simulations investigated how the presence of the manifolds affects the results. The results obtained have shown how the final ^{210}Po concentration is 8% and 7% lower, respectively for the IB and the OB loops, not including the manifolds in

the model.

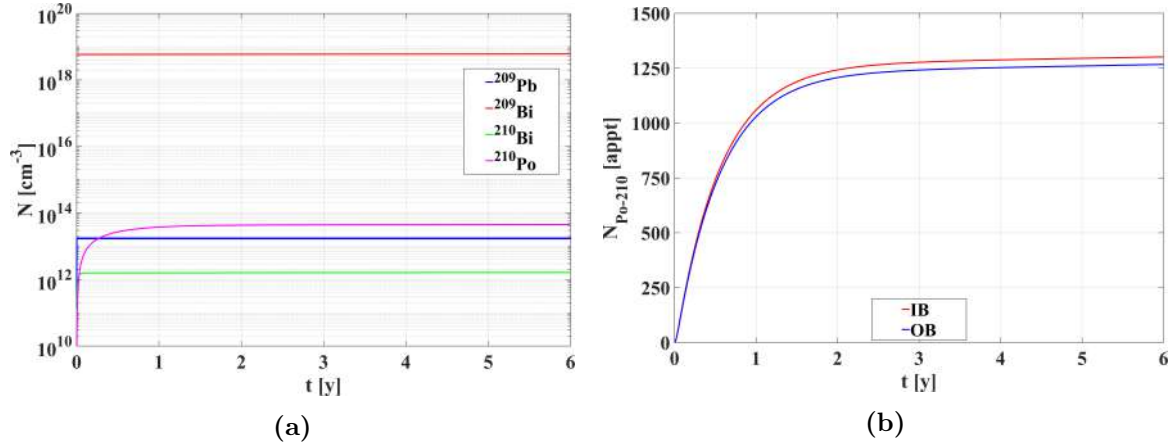


Figure 9: Time behaviour of the average isotope concentrations in the IB PbLi loop (a), and time evolution of the average ^{210}Po concentrations inside the IB and OB PbLi loops (b).

To clarify the effect of the pulsed neutron source on the behaviour of the isotope concentrations, figure 10 shows the details of the average ^{209}Pb concentration during few pulses. It has to be underlined that the attention has been focussed on this isotope because the pulsed source effect is most evident due to its short half-life. Moreover, the average concentrations have been calculated separately for the in-vessel (blanket and manifolds) and ex-vessel sides of the circuits. It can be observed that in both the OB and IB PbLi loops of the reactor, the isotope concentration oscillations have almost the same period as the source and the time profiles are not so smooth (especially along the in-vessel side of the circuit).

Such behaviour is due to the PbLi speed which makes the loop transit time similar to the source period so that those peculiar interference profiles spring up. The dual aspect of this phenomenology is represented by the spatial distribution of the concentrations which show the same, not so smooth, profiles as the time functions (figure 11). In particular, figure 11, shows the 1D profiles of the ^{209}Pb concentration along the IB and OB circuits at 5 different time values, 3 selected during the flat-top phase of the pulse and 2 during the dwell time. Regarding this topic, it should be noted that both the spatial and time distributions relating to the concentration of ^{210}Po are considerably flatter than the case of ^{209}Pb considered as a clarifying example.

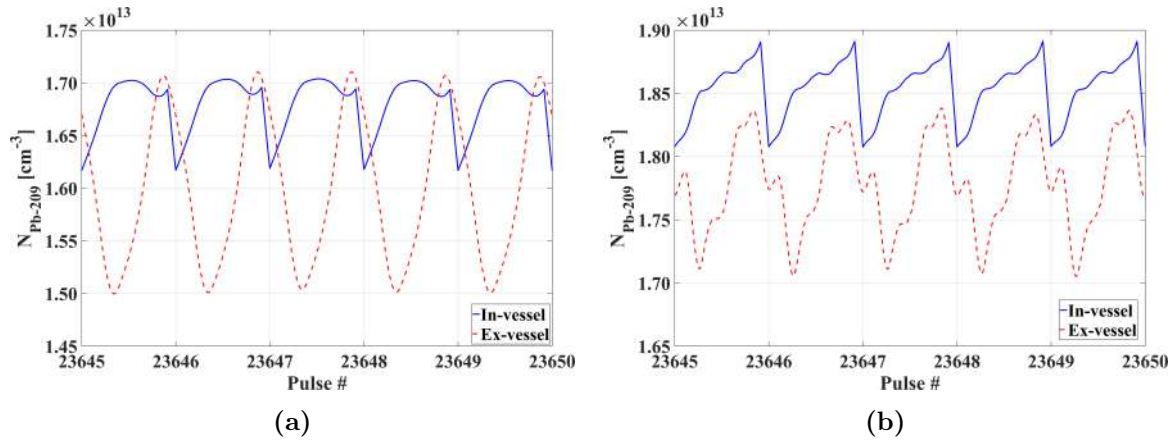


Figure 10: Time evolution of the average ^{209}Pb concentration in the IB PbLi loop (a) and OB PbLi loop (b), reported separately for the in-vessel and ex-vessel components.

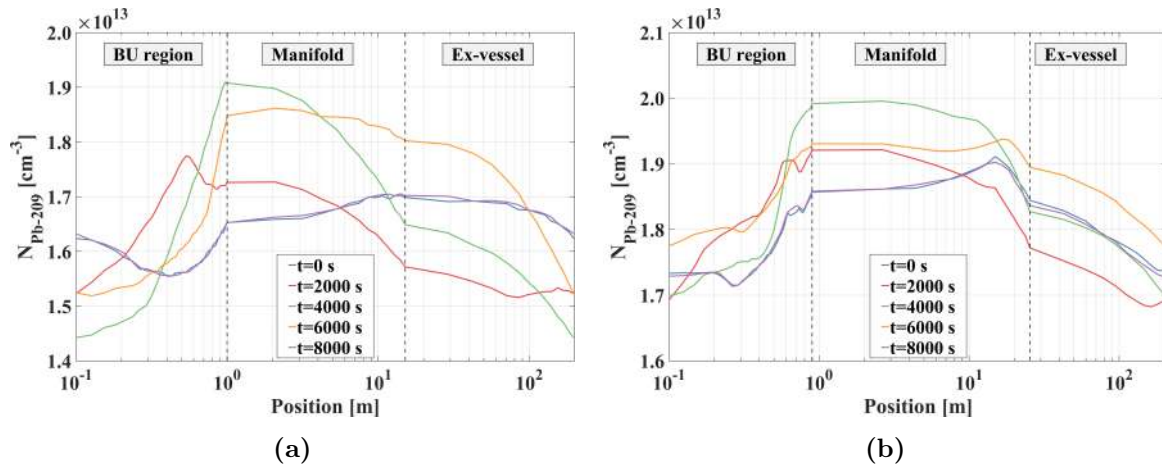


Figure 11: Spatial distribution of ^{209}Pb concentration in the IB PbLi loop (a) and OB PbLi loop (b). Time values reported are relative to the last pulse of the 6 y operation.

Moreover, integrating the ^{210}Po concentration over the volume of each region, it has been obtained the total inventory of this radionuclide, whose breakdown in the circuit is reported in table 4. As it can be argued from the results, a total of ≈ 15 g of ^{210}Po is present inside the entire reactor. Most of it (4.3 g for the IB and 8.8 g for the OB) is present inside the BB, while only less than 2 g are accumulated inside the PbLi ex-vessel pipings and components.

Table 4: ^{210}Po inventories (in grams) after 6 y operation.

	IB	OB
Single BB segment	0.13	0.18
PbLi loop (in-vessel)	2.15	2.20
PbLi loop (ex-vessel)	0.26	0.30
Total (in-vessel)	4.31	8.80
Total (ex-vessel)	0.52	1.22
TOTAL	4.83	10.02

Additionally, a rough sensitivity analysis has been performed to assess the influence on the ^{210}Po inventory of uncertainties related to the branching value (γ) of the ^{209}Bi radiative-capture cross section and the initial concentration of this nuclide ($^{210}\text{Bi}_0$), which is present in the PbLi as an impurity. Regarding the γ value, it cannot be set definitely since different cross section libraries show discrepancies. As far as the ^{209}Bi initial concentration is concerned, its value could vary as it depends on the purity level of the PbLi.

Table 5 and 6 show the inventory of ^{210}Po in both the IB and the OB circuits as γ and $^{209}\text{Bi}_0$ vary, being the reference values $\gamma=2/3$ and $^{209}\text{Bi}_0=170$ appm. It is easy to observe that ^{210}Po concentration varies linearly with γ and grows almost linearly with $^{209}\text{Bi}_0$, so the ^{209}Bi initial concentration is a very important factor to take into account in the WCLL chemistry development. Furthermore, it appears that an experimental campaign is necessary to clarify the uncertainties related to the value of γ .

Table 5: ^{210}Po concentration (in appt) after 6 y operation in IB in-vessel components. **Table 6:** ^{210}Po concentration (in appt) after 6 y operation in OB in-vessel components.

γ	$^{209}\text{Bi}_0$ concentration [appm]				γ	$^{209}\text{Bi}_0$ concentration [appm]			
	0	17	170	1699		0	17	170	1699
0.50	30	125	977	9500	0.50	32	124	952	9226
0.66	40	167	1305	12667	0.66	43	166	1271	12301
1.00	60	250	1955	19001	1.00	65	249	1904	18452

5. Safety considerations

As already noted, the inventory of ^{210}Po might represent a safety problem. The main risk is due to inhalation of ^{210}Po that, accordingly to ICRP [24], has a very low Derived Air Concentration (DAC): with an air breathing rate of $1.1 \text{ m}^3 \text{ h}^{-1}$ DAC is only 3.03 Bq m^{-3} because of its high toxicity and volatility. The main safety issues are relevant to workers, due to the chronic releases and during maintenance (e.g. replacement of components), and to the public in case of accident. The ^{210}Po accumulated in the coolant is mainly restrained as PbPo; only a very minor part ($\approx 10^{-9}$ in [25]) could evaporate into cover gas. The contamination in the air is determined by the aerosol deposition, the surface contamination and the aerosol resuspension. Ventilation combined with the atmosphere

purification system is likely necessary in order to control the ^{210}Po contamination below the limit. From radioactive management point of view, because of its relatively short life, ^{210}Po does not represent a major issue for the radwaste repositories, where the wastes are not delivered before 5 years from the last day of operation. The allowable maximum concentration of ^{210}Po in the air during maintenance can be evaluated according to the following formula:

$$\int_{t_s^w}^{t_e^w} e \frac{A(t)}{V} Q(t) dt \leq D_l \quad (8)$$

where e is the committed effective dose coefficient [26], A is the ^{210}Po activity related to the PbLi leakage, V is the volume of the room in which the maintenance intervention takes place, Q is the air volumetric flow rate inhaled by the worker, and D_l is the effective dose limit foreseen by regulatory authorities. Finally, the limits of integration represent the start and end times of the maintenance intervention. Therefore, since the activity is calculated as the product $\lambda_{Po-210} \cdot N_{Po-210}$, the knowledge of ^{210}Po amount along the PbLi circuit is an important quantity for safety analysis. Another observation can be done taking into account a ^{210}Po concentration limit for safety issues in case of a massive PbLi release following a severe accident. In this sense, safety analyses carried out in [23], starting from evaluations shown in [27], have estimated for DEMO a ^{210}Po limit concentration of 1500 appt in case of interaction between PbLi and air and 100 appt in case of interaction between PbLi and water. ALARA principle has to be applied for occupational exposure and for accidental releases in order to be below the allowable safety limits as reasonably achievable.

As table 5 and 6 show, the maximum of 1305 appt ^{210}Po concentration is calculated in the IB, taking into account the nominal ^{209}Bi initial concentration of about 170 appm which is considered very high in [23]. The assessed maximum ^{210}Po concentration is under the limit evaluated in [23], moreover, it is to be pointed out that this value is very conservative as it has been assessed in the rather artificial scenario described in the previous paragraph.

6. Conclusions

In the framework of the EUROfusion action, a study was conducted to evaluate the inventory and distribution of ^{210}Po in the PbLi circuits envisaged for the DEMO reactor project equipped with a WCLL BB. To this purpose a one-dimensional convective fluid-dynamic model has been developed to solve the Bateman's equations properly modified to consider the alloy circulation, making use of the MCNP code for the calculation of the nuclear quantities involved in the problem. Therefore, both the spatial and time distributions of the concentrations of the isotopes involved in the polonium chain have been assessed.

It has also been found that the initial bismuth concentration plays a crucial role in the production of ^{210}Po , so it seems clear that the purity level of PbLi should be given due consideration. In this context it was also observed that an important parameter for the calculations carried out is the cross section of the radiative capture reaction of bismuth which therefore deserves appropriate investigations aimed at mitigating its uncertainty.

In conclusion, the outcomes obtained supply some rough information for the development of WCLL BB, in terms of ^{210}Po production and transport. So, the results shown could represent a starting point for more refined out-and-out safety investigations related to ^{210}Po . More in general, the numerical method developed could be used also to similar investigations on the radiotoxic waste envisaged for this line of blanket.

Disclaimer

This work has been carried out within the framework of the EUROfusion Consortium and has received funding from the Euratom research and training programme 2014-2018 and 2019-2020 under grant agreement No 633053. The views and opinions expressed herein do not necessarily reflect those of the European Commission.

References

- [1] T. Donné and W. Morris. *European Research Roadmap to the Realisation of Fusion Energy*. 2018. ISBN: 978-3-00-061152-0.
- [2] G. Federici, C. Bachmann, L. Barucca, W. Biel, L. Boccaccini, R. Brown, C. Bustreo, S. Ciattaglia, F. Cismondi, M. Coleman, V. Corato, C. Day, E. Diegele, U. Fischer, T. Franke, C. Gliss, A. Ibarra, R. Kembleton, A. Loving, F. Maviglia, B. Meszaros, G. Pintsuk, N. Taylor, M.Q. Tran, C. Vorpahl, R. Wenninger, and J.H. You. DEMO design activity in Europe: Progress and updates. *Fusion Engineering and Design*, 136:729–741, 2018.
- [3] A. Del Nevo and P. Arena. *BB.WCLL-JUS-2-CD1-BB WCLL Design Description Document (DDD)*. 2021. EUROfusion IDM Ref.: 2NGB4U.
- [4] A. Del Nevo, P. Arena, G. Caruso, P. Chiovaro, P.A. Di Maio, M. Eboli, F. Edemetti, N. Forgiione, R. Forte, A. Froio, F. Giannetti, G. Di Gironimo, K. Jiang, S. Liu, F. Moro, R. Mozzillo, L. Savoldi, A. Tarallo, M. Tarantino, A. Tassone, M. Utili, R. Villari, R. Zanino, and E. Martelli. Recent progress in developing a feasible and integrated conceptual design of the WCLL BB in EUROfusion project. *Fusion Engineering and Design*, 146:1805–1809, 2019.
- [5] C. Bachmann, S. Ciattaglia, F. Cismondi, T. Eade, G. Federici, U. Fischer, T. Franke, C. Gliss, F. Hernandez, J. Keep, M. Loughlin, F. Maviglia, F. Moro, J. Morris, P. Pereslavytsev, N. Taylor, Z. Vizvary, and R. Wenninger. Overview over DEMO design integration challenges and their impact on component design concepts. *Fusion Engineering and Design*, 136:87–95, 2018.
- [6] G. Federici, L. Boccaccini, F. Cismondi, M. Gasparotto, Y. Poitevin, and I. Ricipito. An overview of the eu breeding blanket design strategy as an integral part of the demo design effort. *Fusion Engineering and Design*, 141:30–42, 2019.
- [7] The MathWorks, Inc. *MATLAB Primer*. 2020. Release: R2020b.
- [8] X-5 Monte Carlo Team. *MCNP – A General Monte Carlo N-Particle Transport Code, Version 5*. LANL, Los Alamos, New Mexico, USA, 2003 (April 2003).
- [9] JEFF3.3 nuclear data library. <https://www.oecd-nea.org/dbdata/jeff/jeff33/#neutron>.

- [10] A.J. Koning, D. Rochman, J.-Ch. Sublet, N. Dzysiuk, M. Fleming, and S. van der Marck. TENDL: Complete Nuclear Data Library for Innovative Nuclear Science and Technology. *Nucl.Data Sheets*, 155:1–55, 2019.
- [11] R.B. Firestone. *Table of Isotopes, 8th edition*. Wiley, 1999. ISBN: 978-0-471-35633-2.
- [12] *Liquid Metal Coolants for Fast Reactors Cooled by Sodium, Lead and Lead-Bismuth Eutectic*. Number NP-T-1.6 in Nuclear Energy Series. INTERNATIONAL ATOMIC ENERGY AGENCY, Vienna, 2012.
- [13] N. J. Hoffman, K. A. Murray, J. A. Blink, W. R. Meier, and W. F. Vogelsang. Polonium Aspects Associated with the Use of Lead-Lithium Blankets in Fusion Applications. *Fusion Technology*, 8(1P2B):1376–1384, 1985.
- [14] T. Mitrovic A. Del Nevo, M. Oron-Carl. *Internal Deliverable BB-3.2.1-T007-D001: WCLL BB design and Integration studies 2020 activities*. 2021. EUROfusion IDM Ref.: 2NTP7J.
- [15] A. Venturini M. Utili, M. Oron-Carl. *Internal Deliverable BB-5.1.1-T003-D002: WCLL LiPb DDD - final version 2020*. 2021. EUROfusion IDM Ref.: 2NVZZ7.
- [16] U. Fischer and Y. Qiu. *Material compositions for PPPT neutronics and activation analyses*. 2019. EUROfusion IDM Ref.: 2MM3A6 v1.1.
- [17] Sergei Zimin. A Simplified Analytical Method to Estimate the Bismuth Build-Up and the Polonium Activity in LiPb-Bearing Blankets of a Fusion Reactor. *Fusion Technology*, 26(2):153–167, 1994.
- [18] L. Barucca, E. Bubelis, S. Ciattaglia, A. D’Alessandro, A. Del Nevo, F. Giannetti, W. Hering, P. Lorusso, E. Martelli, I. Moscato, A. Quartararo, A. Tarallo, and E. Vallone. Pre-conceptual design of EU DEMO balance of plant systems: Objectives and challenges. *Fusion Engineering and Design*, 169:112504, 2021.
- [19] F. Moro, P. Arena, I. Catanzaro, A. Colangeli, A. Del Nevo, D. Flammini, N. Fonnesu, R. Forte, V. Imbriani, G. Mariano, R. Mozzillo, S. Noce, and R. Villari. Nuclear performances of the water-cooled lithium lead DEMO reactor: Neutronic analysis on a fully heterogeneous model. *Fusion Engineering and Design*, 168:112514, 2021.
- [20] Pavel Pereslavl'tsev, Francisco A. Hernández, Guangming Zhou, Lei Lu, Christian Wegmann, and Ulrich Fischer. Nuclear analyses of solid breeder blanket options for DEMO: Status, challenges and outlook. *Fusion Engineering and Design*, 146:563–567, 2019.
- [21] P. Chiovaro, S. Ciattaglia, F. Cismondi, A. Del Nevo, P.A. Di Maio, G. Federici, C. Frittitta, I. Moscato, G.A. Spagnuolo, and E. Vallone. Investigation of the DEMO WCLL Breeding Blanket Cooling Water Activation. *Fusion Engineering and Design*, 157:111697, 2020.
- [22] J.R. Dormand and P.J. Prince. A family of embedded Runge-Kutta formulae. *Journal of Computational and Applied Mathematics*, 6(1):19–26, 1980.
- [23] Merlijn A.J. Mertens, Ulrich Fischer, Pavel Pereslavl'tsev, Robert Stieglitz, Jean-Marie Noterdaeme, and Stefaan Cottenier. Po-210 production in the european DEMO fusion reactor. *Nuclear Fusion*, 59(10):106029, 2019.
- [24] RH Clarke, FA Fry, JW Stather, and GAM Webb. 1990 recommendations of the international commission on radiological protection. *Documents of the NRPB*, 4(1):1–5, 1993.
- [25] Deng Lilin, Wang Yuqing, Zhai Zian, Huang Bochen, Wu Jiewei, He Jianbo, and Ni Muye. Multi-physics model development for polonium transport behavior in a lead-cooled fast reactor. *Frontiers in Energy Research*, 9:365, 2021.
- [26] K. Eckerman, J. Harrison, H-G. Menzel, and C.H. Clement. ICRP Publication 119: Compendium of Dose Coefficients based on ICRP Publication 60. *Annals of the ICRP*, 42(4):e1–e130, 2013.
- [27] D.A. Petti, B.J. Merrill, R.L. Moore, G.R. Longhurst, L. El-Guebaly, E. Mogahed, D. Henderson, P. Wilson, and A. Abdou. ARIES-AT safety design and analysis. *Fusion Engineering and Design*, 80(1):111–137, 2006.